The International Journal of Advanced Manufacturing Technology (2019) 100:333–347
https://doi.org/10.1007/s00170-018-2663-9

ORIGINAL ARTICLE

A physical behavior model including dynamic recrystallization and damage mechanisms for cutting process simulation of the titanium alloy Ti-6Al-4V

D. Yameogo[1] · B. Haddag[1] · H. Makich[1] · M. Nouari[1]

Received: 17 April 2018 / Accepted: 4 September 2018 / Published online: 24 September 2018

Abstract

Titanium and its alloys are attractive materials due to their low density and resistance to high temperature and corrosion. However, these materials are also known for their low machinability that leads to poor surface finish and premature tool wear. When machining such materials, serrated chips are often generated. According to the literature, this is generally due to the material damage and microstructure transformation phenomena. A flow stress modeling that takes into account material damage and dynamic recrystallization (DRX) is proposed to obtain a more realistic cutting process simulation of the titanium alloy Ti-6Al-4V. The Johnson-Mehl-Avrami-Kolmogorov (JMAK) model is used to predict the recrystallized volume fraction involved in the proposed flow stress law. The microstructure evolution influences the material damage and the JMAK DRX initiation criterion is used to introduce this effect. A 2D Lagrangian finite element (FE) formulation is adopted to simulate the orthogonal cutting process. The cutting forces and chip morphology, obtained with the proposed behavior model, are analyzed and compared to those obtained with known tangent hyperbolic (TANH) and Johnson-Cook (JC) behavior models. A good accordance between the proposed model simulations and the experimental results is noticed. The link between recrystallization, damage and chip segmentation has been deeply analyzed.

Keywords Machining Ti-6Al-4V · Physical-based model · Microstructure · Damage · Chip morphology · Cutting force · FE analysis

Nomenclature Material properties

E	Young modulus (GPa)
ρ	Material density (kg/m^3)
α	Thermal expansion coefficient (K^{-1})
λ	Thermal conductivity (W/mK)
C_p	Specific Heat (J/kg K)

Thermo-mechanical variables

$\overline{\sigma}$	Flow stress
ε	Equivalent plastic strain
$\dot{\varepsilon}$	Equivalent plastic strain rate
T	Temperature (°K)

Johnson-Cook model parameters

A	Initial yield stress (MPa)
B	Hardening modulus (MPa)
C	Strain rate dependency coefficient
m	Thermal softening coefficient
n	Strain hardening coefficient
T_0	Reference Temperature (°K)
T_m	Melting Temperature (°K)

Johnson-Cook damage parameters

d_1, d_2, d_3, d_4, d_5	Johnson-Cook damage model parameters

JMAK model parameters

X_{DRX}	Recrystallized volume fraction
Q_{act}	Dynamic recrystallization activation energy (J)
R	Gas constant
ε_{crit}	Critical equivalent plastic strain

✉ M. Nouari
mohammed.nouari@mines-nancy.univ-lorraine.fr

[1] University of Lorraine, LEM3 UMR CNRS 7239, Institut Mines-Telecom, GIP-InSIC, 27 rue d'Hellieule, 88100 Saint-Dié-des-Vosges, France

a_1, h_1, m_1, a_2, a_5,JMAK model constants
h_5, m_5, β_d,k_d

TANH model parameters

a, b,c,d TANH model constants

ZA model parameters

$\Delta\sigma_G$ Additional stress depending on initial microstructure
c_1, c_2, c_3, ZA model constants
c_4, c_5, k

MTS model parameters

$\hat{\sigma}$ Mechanical threshold stress
$\hat{\sigma}_a$ Athermal stress
K Boltzmann constant
g_0 Normalized activation energy
μ Shear modulus
b Burger vector
p, q MTS model constants

Cutting parameters

V_C, f Cutting speed, feed

1 Introduction

Hard titanium and its alloys are used in various industrial applications such as manufacturing of airplane components, biomedical devices, and power instruments due to their remarkable properties such as low density, high tensile strength, resistance to corrosion, and high melting temperature. These materials are used for example in manufacturing of aeronautical turbo-machinery thanks to their ability to operate at high temperatures. They also offer a good resistance to corrosion in biomedical applications such as the design of prostheses. However, hard titanium alloys present a number of machining difficulties caused by their thermo-viscoplastic behavior, induced damage, and chemical and thermal processes [1]. For example, cutting force oscillations are encountered during machining operations of titanium alloys, which introduce tool chatter and vibration leading to premature tool wear and poor surface finish [2, 3]. Another commonly encountered issue during machining of titanium alloys is the temperature localization due to their low thermal conductivity [1]. The comprehension of the cutting mechanisms, especially the material behavior is an important step to optimize and improve the machining processes [4, 5]. Since the thermo-mechanical loads (strain rates up to 20,000 s^{-1} [6]) imposed to the material during machining cannot be completely reproduced by laboratory tests, the analysis of the chips gives many valuables information concerning the material behavior during the cutting process. In the case of the Ti-6Al-4V alloy, studied in this paper, segmented chips are obtained (Fig. 1a). Chip segmentation is generally explained by two different mechanisms, namely, material damage and adiabatic shear banding due to the microstructure transformation.

The cyclic fracture mechanism based on material damage was introduced by Nakayama [7] to explain the chip segmentation. This author considered that a periodic crack initiation is responsible of the chip morphology modification. The crack initiates at the chip free surface where the hydrostatic pressure is zero and propagates during chip formation toward the tool tip, creating a shear band. The obtained saw tooth shape of the segmented chip results from the material sliding along this shear band. Shaw and Vyas [8] proposed this mechanism of cyclic fracture to explain the segmentation of a carburized steel. Umbrello [9] predicted chip segmentation in a 2D FE model using the Cockroft and Latham's damage criterion to produce crack propagation. Aurich and Bil [10] used the crack initiation theory to simulate segmentation with a 3D FE model.

The second mechanism to explain the chip segmentation is the formation of adiabatic shear bands (ASB) which are characterized by severe localized plastic deformation. The adiabatic shear bands are the areas of the chip where severe plastic deformation is localized because of the material softening. The ASB propagates from the tool tip to the chip free surface. Zhen-Bin and Komanduri explained in their work [11] that the thermal softening effect in the chip becomes stronger than the strain hardening effect, leading to a thermoplastic instability, a drop of rigidity and finally to the formation of ASB and segmentation. In a similar way, Davies et al. [12] proposed that segmented chips are formed when the cutting speed is too high and breaks the balance between thermal conductivity and plastic deformation. More recent investigations tend to demonstrate that the material softening in the ASB is not only due to thermal softening, but also to microstructural transformation such as phase transformation or dynamic recrystallization (DRX). Wan et al. [13] studied the evolution of microstructure in ASB and observed martensitic phase transformation of β titanium to $\alpha^{''}$ titanium. They also observed grain refinement, which is a characteristic of DRX. Sagapuram et al. [14] observed a transformed nanocrystalline structure in ASB of Ti-6Al-4V chips. Nouari and Makich [15] observed that the grain size in ASB is finer when machining the aeronautical Ti-6Al-4V alloy. Based on experimental investigations, several papers ([16–18]) tend to associate the DRX to the material softening in the ASB and then to the chip segmentation when machining Ti-6Al-4V. Based on this experimental observation of DRX, many modeling approaches are proposed in literature. Rhim and Oh [16] studied the formation of segmented chip using numerical simulation and proposed a material model taking into account the microstructural change in the chip. They explained that the DRX is accompanied by a strong thermal softening which is responsible of the plastic strain localization in ASB. Calamaz et al. [17] also introduced DRX in a

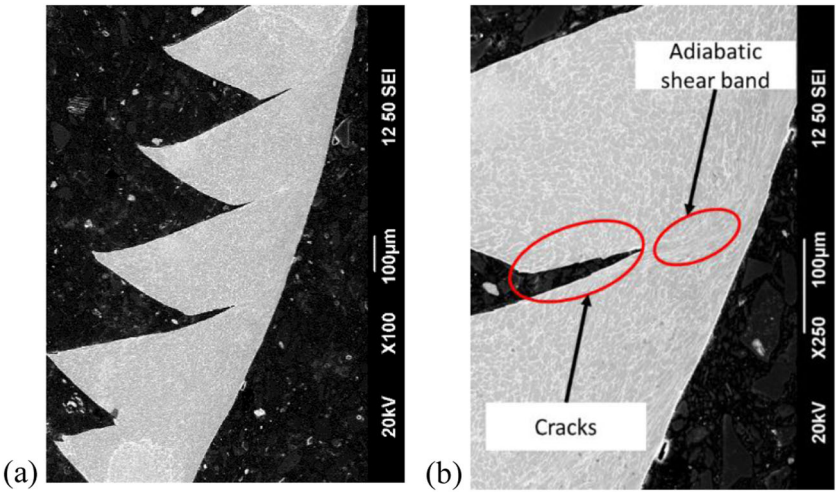

Fig. 1 Ti-6Al-4V chip obtained with $f = 0.35$ mm/rev and $V_c = 25$ m/min. **a** SEM micrograph, magnification × 100. **b** SEM micrograph, magnification × 250

numerical model to predict the chip segmentation when machining the Ti-6Al-4V alloy. Sima and Ozel [19] proposed different improvements of Calamaz's model. However, all these models are based on DRX thermal softening and do not take into account the damage mechanisms. Indeed, their model do not predict the crack initiation which characterize segmented chips of the Ti-6Al-4V alloy.

Nowadays, the tendency is to consider the contribution of the two mechanisms (damage and microstructure transformation) in the chip formation of the Ti-6Al-4V alloy. Liu et al. [18] considered the contribution of the two mechanisms during the chip formation and proposed a modified Zerilli Armstrong flow stress model taking into account damage and recovery. Wan et al. [13] explained this theory by studying Ti-6Al-4V and pointed out a microstructural changes within the ASB. This area is often subjected to grain refinement. They concluded by observing the segmentation process for other materials that the two mechanisms generally contribute together during the formation of segmented chip. This last case is often observed (Fig. 1b). However, there are few modeling strategies proposed in the literature that take into account both damage and DRX mechanism to simulate the cutting process.

In this paper, the cutting process of the titanium alloy Ti-6Al-4V is studied. A physical behavior model is proposed based on two key points. The first point is to consider the difference of the material behavior in the recrystallized and non-recrystallized areas of the chip. A recrystallization criterion based on the Johnson-Mehl-Avrami-Kolmogorov (JMAK) model is introduced to detect the occurrence of DRX. The flow stress is calculated using the recrystallized volume fraction. The second key point is to consider the damage and recrystallization mechanisms in the chip formation and to introduce the effect of DRX on the damage behavior. Then orthogonal cutting is numerically simulated based on the experimental results taken from the literature [20]. Four material behavior models are compared to understand the physics of the cutting process. The cutting forces and the chip morphology are analyzed. Thus, a discussion is conducted on the relationship between chip segmentation, dynamic recrystallization, and damage.

Since the material is submitted to high temperatures, intense loads and high deformation rates during machining operations, material constitutive laws play an important role in cutting process simulation. In addition to this, the microstructure evolution is more and more taken into account in flow stress models. For example, Atmani et al. [21] studied the chip formation process of the OFHC copper through a 2D finite element modeling considering microstructure changes. They used the mechanical threshold stress model and the dislocation density model to predict the chip morphology and microstructural evolutions. In this section, many material behavior models used in machining simulation are recalled. All the models presented here are thermo-viscoplastic models and thus the variables ε, $\dot{\varepsilon}$, and T, which are the plastic strain, plastic strain rate and temperature, respectively are considered. We distinguish two kinds of flow stress models.

1.1 Phenomenological based flow stress models

Phenomenological models are based on experimental observations and present the advantage of being easy to set up. A well-known example of these models is the Johnson-Cook (JC) flow stress law. It is generally used to represent dynamic behavior of ductile metals and is very applied to simulate perforation of metals or hot compression process. The model parameters are usually determined with the Split-Hopkinson pressure bar test (SHPB). The Johnson-Cook (JC) model is given by Eq. (1) presented in Table 1, where A, B, C, n, m, and p are the model parameters. The first term of Eq. (1) represents the material initial yield stress and strain hardening. The second term which depends on the plastic strain rate represents the hardening due to the deformation rate. It is known that increasing the strain rate tends to raise the flow stress. The last

Table 1 Material behavior flow stress models

Model	Equation
JC	$\overline{\sigma} = (A + B\varepsilon^n)\left(1 + C\left[\ln\left(\frac{\dot{\varepsilon}}{\dot{\varepsilon}_0}\right)\right]\right)\left(1-\left(\frac{T-T_0}{T_m-T_0}\right)^m\right)$ (1)
TANH	$\overline{\sigma} = \left[A + B\varepsilon^n\left(\frac{1}{\exp(\varepsilon^a)}\right)\right]\left[1 + C\ln\frac{\dot{\varepsilon}}{\dot{\varepsilon}_0}\right]\left[1-\left(\frac{T-T_0}{T_m-T_0}\right)^m\right]\left[D + (1-D)\tanh\left(\frac{1}{(\varepsilon+S)^c}\right)\right]$ (2) with $D = 1-\left(\frac{T}{T_m}\right)^d$ (3) and $S = \left(\frac{T}{T_m}\right)^b$ (4)
MTS	$\overline{\sigma} = \hat{\sigma}_a + (\hat{\sigma}-\hat{\sigma}_a)\left\{1-\left[\frac{KT\ln\left(\frac{\dot{\varepsilon}_0}{\dot{\varepsilon}}\right)}{g_0\mu b^3}\right]^{\frac{1}{q}}\right\}^{\frac{1}{p}}$ (5)
ZA	$\overline{\sigma} = \Delta\sigma_G + c_1\exp(-c_3T + c_4T\ln\dot{\varepsilon}) + c_5\varepsilon^n + kl^{-1/2}$ (6) $\overline{\sigma} = \Delta\sigma_G + c_2\varepsilon^{1/2}\exp(-c_3T + c_4T\ln\dot{\varepsilon}) + kl^{-1/2}$ (7)
Enhanced ZA	$\overline{\sigma} = \left[\sigma_a + B\exp(-\beta_0T + \beta_1T\ln\dot{\varepsilon}) + B_0\sqrt{\varepsilon_r(1-\exp\left(\frac{-\varepsilon}{\varepsilon_r}\right)}\exp(-\alpha_0T + \alpha_1T)\right]\left[H^* + \left(1-H^*\right)\left(\tanh\left(\frac{a^*}{\varepsilon}\right)\right)^{k^*}\right]$ (8)

term depends on temperature and represents thermal softening. All these phenomena appear during machining and justify the use of such models.

As recalled in the introduction, microstructural modifications like recrystallization, restoration, or phase transformation are observed during machining operations. Recrystallization is characterized by finer grain size in the machined sub-surface and in the chip. In materials like Ti-6Al-4V, DRX is observed in ASB and is accompanied by material softening [19]. This softening effect is often observed during compression and hot deformation tests (Fig. 2).

Calamaz et al. [17] built up a model by modifying the JC model to introduce the microstructural effect called "strain softening" by adding a tangent hyperbolical term. They obtained a segmented chip from their simulations but they did not reproduce the damage phenomenon, namely the crack formation. This model is given by Eqs. (2), (3) and (4), where A, B, C, n, m, p, a, b, c, and d are the model parameters.

1.2 Physical-based flow stress models

Metal plasticity physical models are based on the dislocation theory which was introduced since 1934 with the works of Orowan, Polanyi, and Taylor. According to this theory, dislocation sliding is responsible of the relative displacement of crystalline planes, resulting in plastic deformation. A well-known physical model is the mechanical threshold stress (MTS) model introduced by Follansbee and Kocks [22]. The mechanical threshold stress is a reference stress corresponding to the flow stress at a temperature of 0 K and is used as an internal state variable in the model. The flow stress is calculated as an addition of an athermal stress and a thermally activated stress. The athermal part characterizes the rate independent interactions of dislocations with long-range obstacles. The thermal part of the equation describes the rate dependent interactions with short range obstacles. The full model is

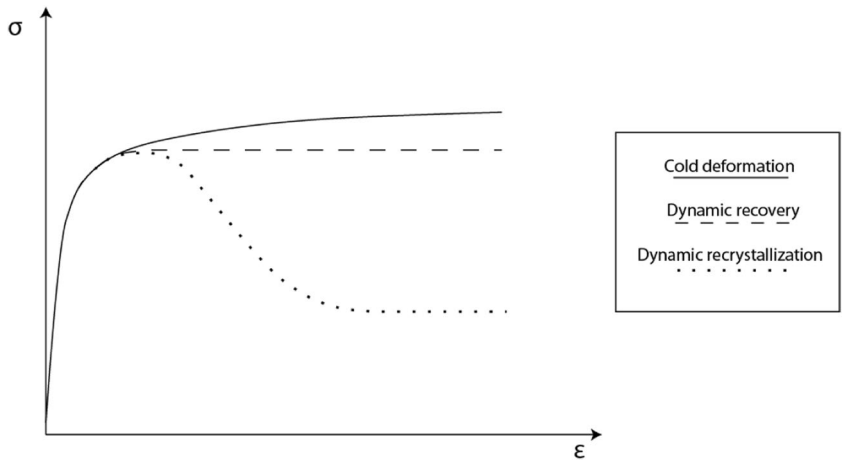

Fig. 2 Scheme of dynamic recovery and recrystallization effects on flow curves

described in reference [22]. Atmani et al. [21] used this model to predict the chip formation in orthogonal cutting configuration for machining simulation. The model is given by Eq. (5) of Table 1.

Zerilli and Armstrong (ZA) [23] built up a constitutive material flow stress model based on dislocations theory. Equations (6) and (7) represent the ZA model [23]. Equation (6) is used for metals with a body-centered cubic (BCC) crystal structure and Eq. (7) for those with faced-centered cubic (FCC) crystal structure. There are two equations because dislocations movement thermal activation is different depending on the crystallographic structure. $\Delta\sigma_G$is an additional component of stress which represents the influence of the material solute and initial dislocation density. k is a microstructural stress intensity and l the average grain diameter. When the average grain size is small, there are more grain boundaries. These grain boundaries are obstacles to dislocations displacement. This resistance is introduced by the stress increment$kl^{-1/2}$in Eq. (6) in which c_1, c_2, c_3, c_4, and c_5 are the model parameters. This model is physical based and reproduces thermal softening, strain, and strain rate hardenings and takes into account the crystal structure and grain size.

Liu et al. [18] proposed a modified ZA model by adding a multiplicative term in order to introduce the effect of damage. This model was built considering that segmented chips are formed due to dynamic recovery (DRV) but also to damage. According to them, these two mechanisms are responsible of the softening during Ti-6Al-4V segmentation process. Equations (6) and (7) have been written differently to form one modified equation and to introduce DRV and damage as given by Eq. (8). In this equation, σ_a is an athermal stress due to initial microstructure in term of grain boundaries and solute atoms. The first term of the equation characterizes recovery through ε_r, a characteristic strain which represents recovery occurrence. B, B_0, β_0, and β_1 are material parameters. The second term with the parametersH^*, a^*, and k^* allows to consider damage due to cracks and micro voids. The enhanced ZA model is interesting but considering that damage and DRX occur in the same time in the same location in the material is not correct, since these physical mechanisms are antagonist. This point is discussed in the present work.

The reported models in Table 1 has their limits when applied to simulate the cutting process of titanium alloy Ti-6Al-4V. These models do not reproduce correctly the cutting process of Ti-6Al-4V. Indeed, it is observed in the ASB, giving rise to segmented chips, a partial fracture starting from the chip free surface and inward the ASB there is intense localized deformation with material transformation and without any damage. Hence, a physical behavior model, based on combining two flow stresses, is proposed in this paper. The physical aspects of this model are in the introduction of a material transformation criterion based on the JMAK model to distinguish between transformed and non-transformed zones, and where damage behavior is attributed.

2 Multi-physic modeling of machining the hard Ti-6Al-4V alloy

2.1 Motivation

Damage mechanism and microstructure transformation have been identified during the chip formation when machining the hard alloy Ti-6Al-4V. These mechanisms modify the material behavior and many studies were conducted on this topic. Damage and microstructural transformations soften the material which results in chip segmentation. However, these two mechanisms are very different and do not occur under the same conditions. High temperature induces microstructural transformation while damage mechanisms occur faster at low temperature. Instead of considering the two mechanisms, most of the simulations in literature takes into account either the damage mechanism or the microstructure transformation to model the cutting process since it is sufficient to reproduce the segmentation of the chip. In addition, ductile damage models are often used without taking into account the influence of microstructure transformation.

In fact, microstructure transformation, like DRX, impedes the occurrence or the evolution of damage mechanisms, which results in high plastic deformation. It is therefore important to take into account the thermo-mechanical conditions influence on the occurrence of damage or microstructure transformation, to reproduce more accurately the material cutting process. For this purpose, a modeling approach that takes into account both damage mechanism and microstructure evolution is built by introducing DRX initiation criterion and microstructure evolution variable. The JMAK model is used for this purpose. So the proposed model, named hybrid model, involves two parts depending on microstructure evolution: a flow stress affected by damage and a flow stress affected by microstructure transformation.

2.2 Proposed hybrid model

2.2.1 Flow stress model

Figure 3a is a scanning electron microscope (SEM) micrograph of a Ti-6Al-4V chip which reveals its microstructure and the distribution of the plastic deformation. The β phase grains appear in white while the α phase grains appear in gray. It can be seen that the plastic strain distribution is heterogeneous with deformed and un-deformed areas. A

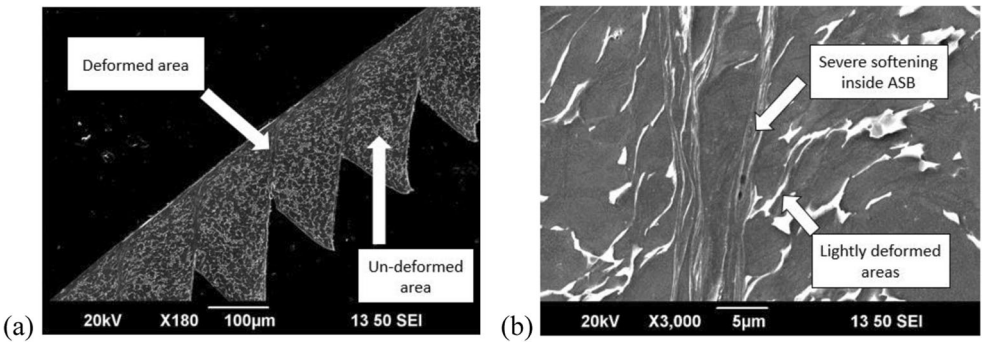

Fig. 3 SEM micrographs of the Ti-6Al-4V chip obtained with machining conditions of 0.18 mm for feed and 150 m/min for cutting speed: **a** Chip morphology and **b** microstructure around the ASB

finer observation is given by Fig. 3b and shows that there are lightly deformed areas close to the ASB and severe deformed areas inside. The intensity of the plastic defor mation can be estimated by an observation of the β grains length and thickness. The more they are thin and long, the more the material underwent plastic deformation.

Two key points guide the construction of the proposed modeling. The first, developed hereafter, is to consider that the physical mechanisms occurring during the cutting process are different depending on the area considered in the chip. The second, developed in Section 2.2.2, is to consider a competition between damage and recrystallization mechanisms at the local scale (i.e., at the material point).

The lightly deformed material is affected by thermal softening, strain hardening, and strain rate effect. In these areas, there is no notable effect of microstructure transformation since the material is lightly deformed. However, in the severely deformed areas, where DRX have been observed by many authors ([13–15]), the dislocation density decreases and therefore, the material flow stress undergoes an important drop (Fig. 2), leading to a low rigidity and a localization of plastic strain. There are different types of DRX, namely the discontinuous, continuous, and geometric DRX. The type of DRX mainly depends on the stacking fault energy of the material, the thermo-mechanical conditions and the initial grain size. Discontinuous DRX is characterized by new grains nucleation and grain growth. The resulting microstructure presents generally a low density of dislocations. In the case of the machining Ti-6Al-4V, many observations ([13–15]) show a fine microstructure with submicrometric grains, which can be regarded as a consequence of discontinuous DRX. Thus, the assumption that the DRX is discontinuous during Ti-6Al-4V chip formation is made in this work and the JMAK model, which is a model for the discontinuous process, is adopted.

Therefore, the JMAK model recrystallization criterion is introduced to detect the thermo-mechanical conditions allowing the occurrence of DRX. When the plastic strain is higher than the critical plastic strain ($\varepsilon \geq \varepsilon_{crit}$), the material starts to recrystallize. ε_{crit} is calculated according to the reference [24] and is given by Eq. (9). a_1, m_1, and a_2, are the model parameters. Q_{act} is the activation energy. R is the gas constant. The initial values of the parameters are chosen from references [24, 25] and fitted. These parameters are gathered in Table 2.

$$\varepsilon_{crit} = a_2 a_1 \dot{\varepsilon}^{m1} \exp\left(\frac{Q_{act} m_1}{RT}\right) \tag{9}$$

The recrystallized volume fraction X_{DRX} is given by Eq. (10). Its value varies from 0 corresponding to the initial state of the material before the DRX occurrence, to 1 which corresponds to a state where the material volume is completely recrystallized. a_5, m_5, β_d, and k_d are the model parameters summarized in Table 3. The initial values of the parameters are chosen from references [24, 25] and fitted.

$$\begin{aligned} &X_{DRX} = 1 - \exp\left[-\beta_d \left(\frac{\varepsilon - \varepsilon_{crit}}{\varepsilon_{0.5}}\right)^{k_d}\right] \text{ if } \varepsilon \geq \varepsilon_{crit} \\ &\dot{X}_{DRX} = 0 \text{ if } \varepsilon < \varepsilon_{crit} \\ &\text{with } \varepsilon_{0.5} = a_5 \dot{\varepsilon}^{m5} \exp\left(\frac{Q_{act} m_5}{RT}\right) \end{aligned} \tag{10}$$

Table 2 JMAK model parameters for recrystallization critical strain

	a_1	m_1	a_2	Q_{act} (kJ mol^{-1})	R (J K^{-1} mol^{-1})
Adopted parameters	0.8	0.01	0.4	218	8.31
Arisoy and Ozel [24]	2	0.006	0.8	218	8.31
Pan et al. [25]	0.0064	0.0801	0.8	381.76	8.31

Table 3 JMAK model parameters for DRX kinetics

	a_5	m_5	β_d	k_d
Adopted parameters	0.022	0.03	2	2
Arisoy and Ozel [24]	1.21 10^{-5}	0.04	0.693	2
Pan et al. [25]	0.022	0.11146	0.9339	0.5994

Table 4 JC and TANH models parameters

	A (MPa)	B (MPa)	C	m	n	$\dot{\varepsilon}_0$ (s^{-1})	a	b	c	d
Adopted parameters	968	380	0.02	0.577	0.421	1	1.6	0.4	6	*0.5*
Ducobu et al. [20]	968	380	0.02	0.577	0.421	1	1.6	0.4	6	*1*

Two flow stresses, corresponding to the cases where $X_{DRX}$is equal to 0 and 1, are considered. When $X_{DRX}$is equal to 0, the material follows a thermo-viscoplastic behavior. When $X_{DRX}$is equal to 1, the material has a thermo-viscoplastic behavior affected by a softening caused by DRX. For intermediary cases, the flow stress depends on the recrystallized volume fraction. Therefore, the material flow stress is calculated as a weighted sum (Eq. (11)) of the two flow stresses described previously. The flow stresses for the non-affected areas and the completely recrystallized areas are calculated according to the JC model (Eq. (12)) and the TANH model (Eq. (13)), respectively. A, B, C, n, and m are the JC model parameters. T_0 and T_m are respectively the reference temperature (298 K) and the melting temperature (1878 K). $\dot{\varepsilon}_0$ is the reference strain rate. a, b, c, and d are the TANH model parameters. The parameters for the JC and the TANH models are given in Table 4. The parameter d influences the softening of the flow stress due to the DRX (see Calamaz et al. [17]). d is fitted in this work.

$$\overline{\sigma}_{Hybrid} = (1-X_{DRX})\overline{\sigma}_1 + X_{DRX}\overline{\sigma}_2 \tag{11}$$

$$\overline{\sigma}_1 = (A + B\varepsilon^n)\left(1 + C\left[\ln\left(\frac{\dot{\varepsilon}}{\dot{\varepsilon}_0}\right)\right]\right)\left(1-\left(\frac{T-T_0}{T_m-T_0}\right)^m\right) \tag{12}$$

$$\overline{\sigma}_2 = \left[A + B\varepsilon^n\left(\frac{1}{\exp(\varepsilon^a)}\right)\right]\left[1 + C\ln\frac{\dot{\varepsilon}}{\dot{\varepsilon}_0}\right]\left[1-\left(\frac{T-T_0}{T_m-T_0}\right)^m\right]\left[D + (1-D)\tanh\left(\frac{1}{(\varepsilon+S)^c}\right)\right]$$
$$\text{with } D = 1-\left(\frac{T}{T_m}\right)^d \text{ and } S = \left(\frac{T}{T_m}\right)^b \tag{13}$$

2.2.2 Damage model

As recalled in introduction, damage and DRX are two mechanisms often observed experimentally ([7, 13]) and considered in a large number of Ti-6Al-4V cutting simulations. However, despite the fact that recrystallization increases ductility and reduces damage, this effect is not taken into account by several authors. Ductile damage is accompanied by plastic deformation and then dislocation multiplication driving to a local raise of stress. This increase of the stress is amplified by the presence of inclusions inside the material and results in nucleation of micro-voids. The micro-voids grow and when there are several micro-voids close to each other, coalescence is observed. Finally the accumulation, growth, and coalescence of these micro-defects result in fracture and crack formation. Recrystallization is a process where the material reduces its stored energy and during which one new microstructure appears with a low density of dislocation. The dislocation number is reduced by annihilation or rearrangement mechanisms. During the recrystallization the stress drops and the material undergoes softening.

Recrystallization is used in annealing processes to reduce the damage in the material and thus, when the material undergoes recrystallization, the damage evolution is affected. According to Shang et al. [26], recrystallization impedes micro-voids growth and coalescence mechanisms, which are important processes in damage accumulation. Some damage models taking into account recrystallization are proposed in literature ([27, 28]) and according to them, a damage decrease is observed when restoration or recrystallization occurs (healing).

Based on these considerations, the following approach is proposed for damage modeling of the cutting process. The fracture strain ε_f is estimated according to the Johnson-Cook ductile damage model and depends on strain rate, temperature, and stress triaxiality. The stress triaxiality is the ratio of the hydrostatic pressure P on the equivalent stress $\overline{\sigma}$. The stress triaxiality is calculated according to Eq. (14). d_1, d_2, d_3, d_4, and d_5 are the model parameters taken from the reference [29]. The parameters are recalled in Table 5.

$$\varepsilon_f = \left[d_1 + d_2\exp\left(d_3\frac{P}{\sigma}\right)\right]\left[1 + d_4\ln\left(\frac{\dot{\varepsilon}}{\dot{\varepsilon}_0}\right)\right]\left[1 + d_5\frac{T-T_0}{T_m-T_0}\right] \tag{14}$$

Table 5 Johnson-Cook damage law parameters

	d_1	d_2	d_3	d_4	d_5
Adopted parameters from Wang and Liu [29]	−0.09	0.25	−0.5	0.014	3.87

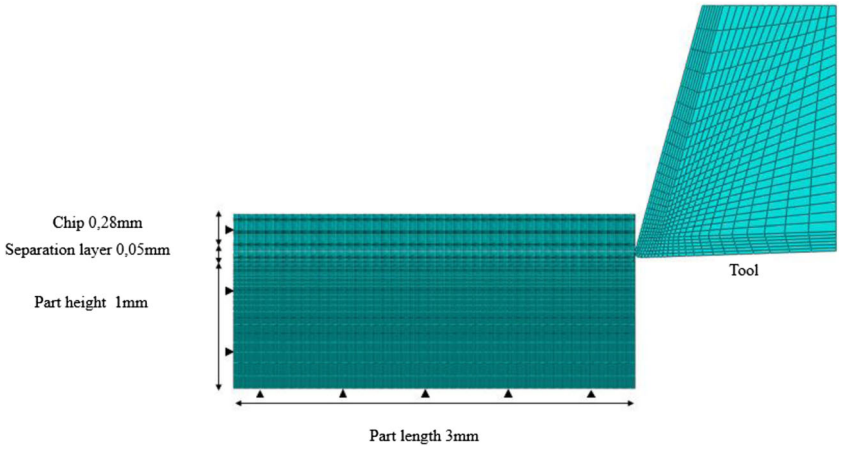

Fig. 4 Orthogonal cutting finite elements model in Lagrangian configuration

As soon as there is the plastic deformation in the material, there is an accumulation of micro-defects leading to the beginning of the material deterioration. This accumulation is estimated by the damage initiation parameter w which varies from 0 to 1. w is calculated according to the following equation:

$$w = \int \frac{d\bar{\varepsilon}_p}{\varepsilon_f} \tag{15}$$

When the damage initiation parameter reaches 1, the material properties starts to be deteriorated and the micro-defects number and size increase until fracture. The criterion chosen for fracture is the Hillerbord's fracture energy criterion. It is described by Eq. (16). G_f is the fracture energy, u_0 and u_f are respectively the plastic displacement at the beginning of material deterioration and the plastic displacement at fracture. σ_y is the flow stress.

$$G_f = \int_{u_0}^{u_f} \sigma_y du \tag{16}$$

The deterioration is measured by the damage variable d, which is equal to 0 when the deterioration begins and is equal to 1 at the fracture occurrence. The damage variable increases with plastic deformation. However, a new condition is introduced to take into account the DRX influence. If there is recrystallization ($\varepsilon \geq \varepsilon_{crit}$), the damage does not increase with further plastic strain. Even if the damage does not increase with plastic deformation during recrystallization, because of the high strain rates in machining it is not considered that the damage decreases. The damage evolves according to the following relation:

$$\dot{d} = \begin{cases} \dfrac{L\dot{\varepsilon}}{u_f} & \text{if } (\varepsilon < \varepsilon_{crit} \text{ and } w = 1) \\ 0 & \text{if } (\varepsilon \geq \varepsilon_{crit} \text{ or } w < 1) \end{cases} \tag{17}$$

where L is the characteristic length of the considered finite element and depends on its size and type.

3 LAG-FE model of orthogonal cutting

The numerical simulation is carried out using Abaqus/explicit code and the Vumat subroutine tool is used to introduce material flow stress and damage behaviors. The simulation is made in a thermo-mechanical frame with a Lagrangian configuration where the workpiece is divided in three parts, namely the non-deformed chip, the separation layer and the part (Fig. 4). This method of the separation layer is adopted in order to reproduce the crack formation in the chip by the element deletion technique. The JC ductile damage model and the Hillerborg's failure criterion, described previously, associated with a FE deletion are used also for the chip separation. The tool is considered as a thermo-rigid body.

The simulated cutting condition is taken from literature and the numerical results are compared with the experimental ones from the reference [20]. A cutting speed of 30 m/min is used for the simulation with a depth of cut of 0.28 mm. The work material is the hard titanium alloy Ti-

Table 6 Mechanical properties of workpiece and tool materials [20]

	E (GPa)	λ (W/mK)	α (K^{-1})	C_p (J/kgK))	ρ (kg/m^3)
Ti-6Al-4V	113.8	7.3	$8.6e^{-6}$	580	4430
Tungsten carbide	800	46	$4.7e^{-6}$	203	15,000

Table 7 Different strategies simulated

Case	Description
Hybrid model	The physical model with flow stress and damage influenced by microstructure evolution
TANH model	Modified JC model with flow stress influenced by microstructure evolution
JC damage model	JC flow stress model with JC damage model
JC damage model with element deletion	JC flow stress model with JC damage model with element deletion to reproduce crack formation

6Al-4V while the tool material is made of tungsten carbide. Mechanical properties of these materials are given in Table 6. The machine is a three milling machine and the cutting tool is fixed on the machine table. The part is mounted in a spindle and moves horizontally. This configuration is adopted to reproduce the orthogonal cutting configuration. The tool has a rake angle of 15°, a clearance angle of 2°, and a cutting edge radius of 20 μm. The friction between the tool and the workpiece is introduced with a Coulomb friction law with a friction coefficient of 0.05. The model is bi-dimensional (2D) since orthogonal cutting conditions are fulfilled, meaning that the tool and the part relative displacement can be described in a plane and the ratio of the chip width on its un-deformed thickness is higher than 3.5, [20].

Four strategies of modeling with different material behaviors are simulated and compared to understand the cutting process. The first model simulated is the hybrid model presented in Section 2.2 and takes into account damage and DRX and the interaction between these two phenomena. The second model simulated is the TANH model described by Eq. (13) and takes into account the material softening due to DRX occurrence. The third model takes into account the JC model and the JC damage model given by Eqs. (12) and (14), respectively. Therefore, the material failure due to damage is reproduced but not the crack initiation in the chip since no element deletion feature is activated in the chip. The fourth model is similar to the third one but element deletion is activated in the chip to reproduce crack formation. These cases are recalled in Table 7. The same parameters, reported in Tables 4 and 5, are used for simulated cases of Table 7.

4 Results and discussion

4.1 Analysis of the chip morphology

The simulation with the hybrid model gives a good morphology accordance between the numerical and the experimental chip as shown in Fig. 5. Both adiabatic shear band and crack initiation observed on the real chip are reproduced by the model.

The performance of the hybrid model is evaluated in comparison with the TANH and JC models. The parameters used to define the chip morphology are L, H, and C (Fig. 5b). The un-deformed chip length L is related to the frequency of chip segment formation. The higher this parameter is, the lower the chip segmentation frequency is. The segmentation frequency F_g depends on L and the the cutting speed according to the following equation:

$$F_g = \frac{V_c}{L} \tag{18}$$

The parameters H and C are respectively the maximum and minimum chip thickness and defines the segmentation intensity. If they are close, the chip is continuous. If the gap between them is high, the chip segmentation is intense (Kouadri et al. [30]). These parameters are measured for the all simulations and compared to the experimental data ([20]) in Table 8.

Figure 6 shows the chip morphology obtained with the four numerical simulations. The results show that the hybrid model (Fig. 6a) produces a chip morphology closer to the experimental one than the other models and reproduce well the plastic strain localization and the crack initiation. As expected, the

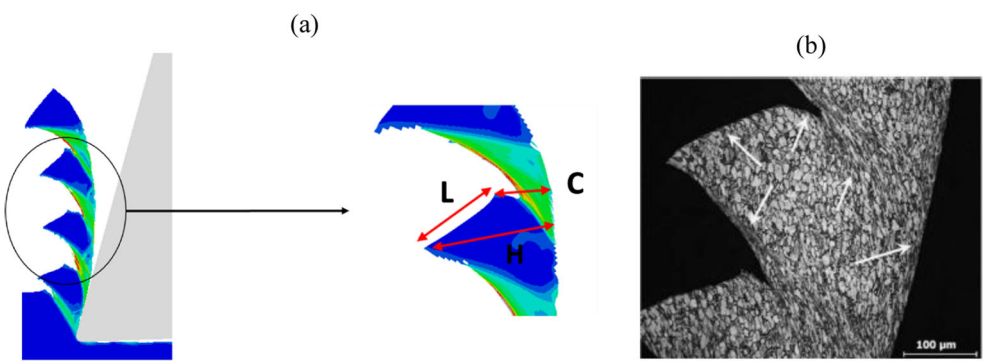

Fig. 5 **a** Numerical chip obtained with hybrid model and **b** experimental chip [17] (V_c=30 m/min and f=0.28 mm/rev)

Table 8 Chip morphology parameters: comparison between experimental data and predictions with different models (V_c=30 m/min and f=0.28 mm/rev)

n	H (μm)	C (μm)	L (μm)	F_g (Hz)
Hybrid model	321 ± 5.8	164 ± 9.2	189 ± 2	2641
TANH model	286 ± 32	183 ± 32	160 ± 18	3164
JC damage model	280 ± 4.5	205 ± 18	110.7 ± 12	4570
JC damage model with element deletion	222 ± 20	0 ± 0	96 ± 14	5328
Experimental [20]	288 ± 14	157 ± 21	206 ± 17	2427

TANH model (Fig. 6b) reproduces the segmentation but not the crack initiation observed on the real chip, since this model does not take into account damage. The JC damage model (Fig. 6c) also reproduces segmentation but no crack since the element deletion feature is not activated. Finally, the JC damage model associated with element deletion feature (Fig. 6d) produces a discontinuous chip because the crack appears at the tool tip and propagates until the chip free surface. On the real chip, the crack initiation occurs at the chip free surface and propagates toward the tool tip. This observations show that the hybrid model reproduces better the chip formation process than the other models.

The comparison of the simulations with the experimental results for the segmentation frequency (Eq. (18)) and the morphology parameters are presented in Table 8, and these results show that the hybrid model gives the best morphology. H and C are well predicted by the hybrid and the TANH models. Hence, the shape of the numerical chips predicted with these two models is similar to the experimental ones. For the simulation with the JC damage models, these parameters are predicted with an important error when compared to experimental results. The JC model without element deletion feature produces a numerical chip with less segmentation. The JC model with deletion element chip is discontinuous and fragmented. For L only, the hybrid model gives a good prediction. The segmentation frequency F_g is therefore well predicted. For the other models, L value is too low and therefore the segmentation frequency is too high in comparison to the experimental results. It is interesting to point out that Ducobu et al. [20] obtained an important error for the same parameters when using TANH to predict chip morphology for the same

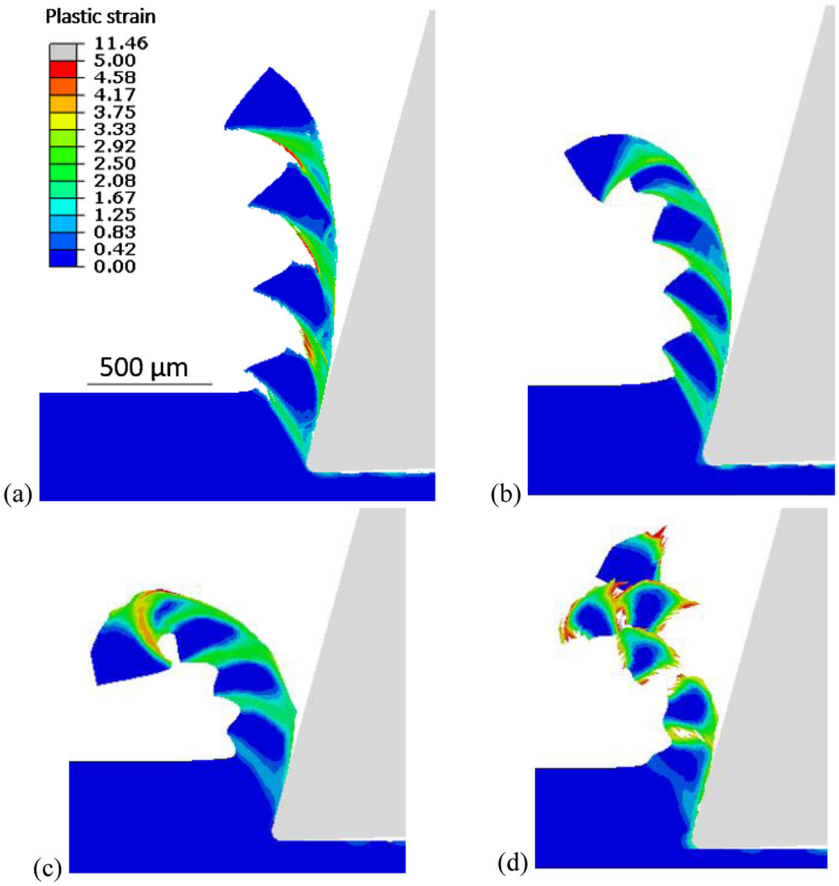

Fig. 6 Chip morphology obtained for V_c=30 m/min and f=0.28 mm/rev: **a** Hybrid, **b** TANH, **c** JC damage, and **d** JC damage with FE deletion models

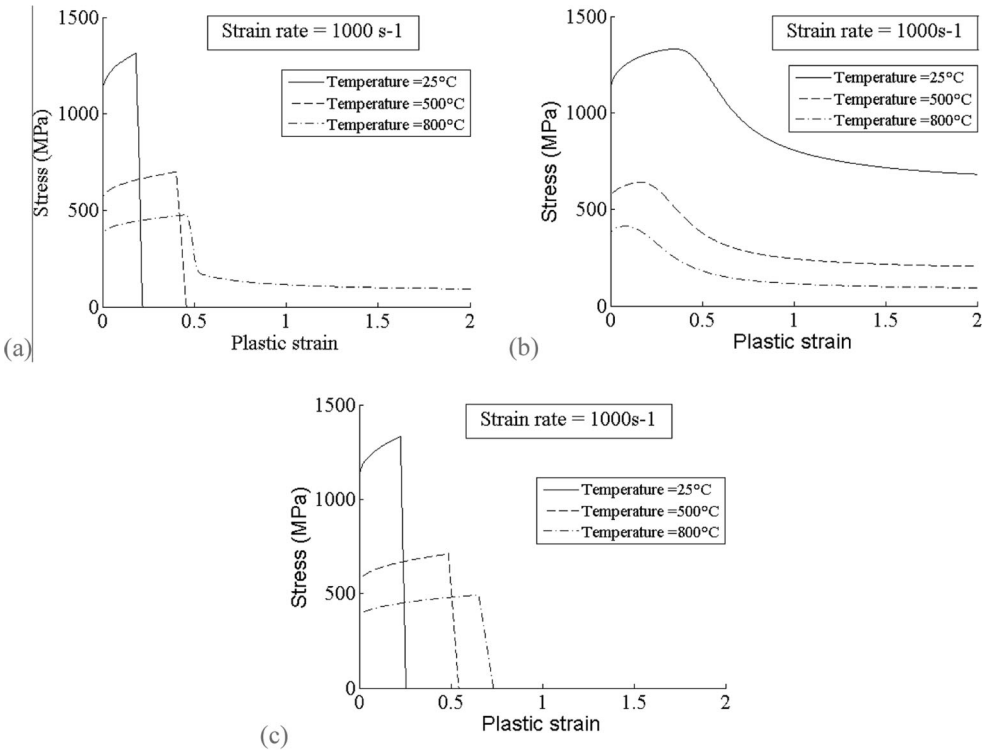

Fig. 7 Flow stress curves. **a** Hybrid. **b** TANH. **c** JC Damage models

material and cutting condition. The TANH and the JC damage models reproduce segmentation but not the fracture in the chip. Finally, the JC damage model associated with element deletion produce fracture with a crack initiation at the tool of the chip while the experimental observations show an initiation at the chip free surface. These results are in accordance with the assumptions previously made and confirm that recrystallization has an effect on damage process. Figure 7 shows the flow stress curves for each model. The softening of the Hybrid model appears for a higher

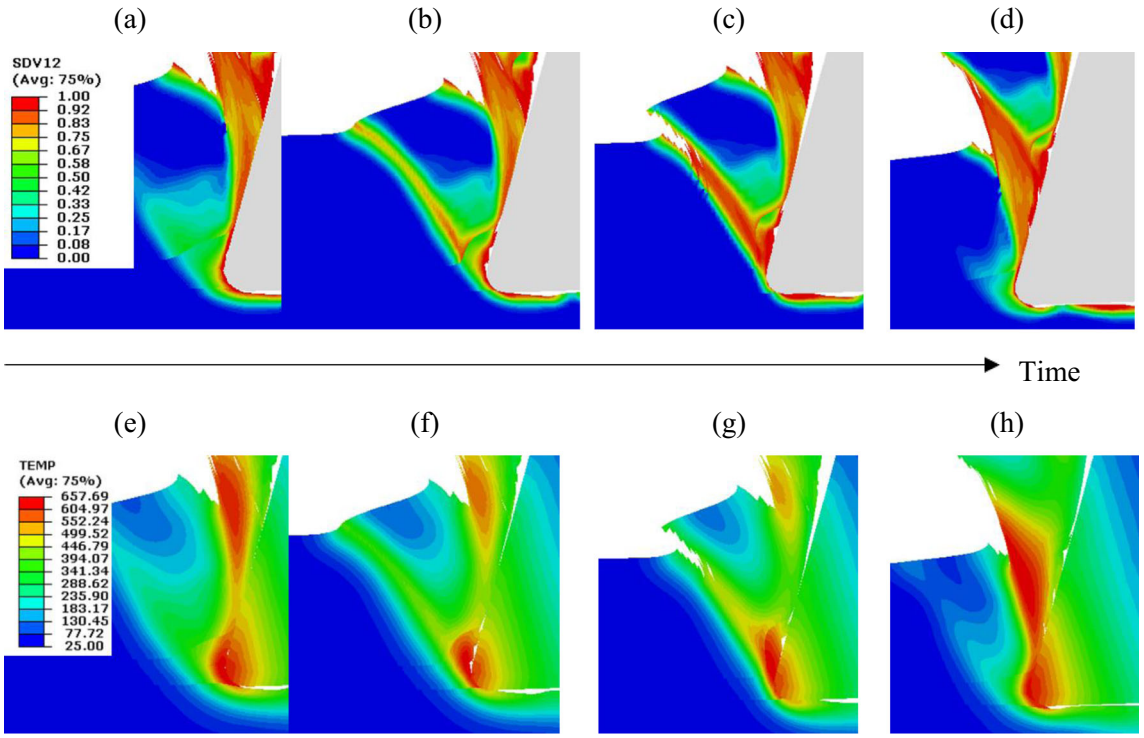

Fig. 8 Simulated cutting process with hybrid model. **a**–**d** damage variable and **e**–**h** temperature (°C)

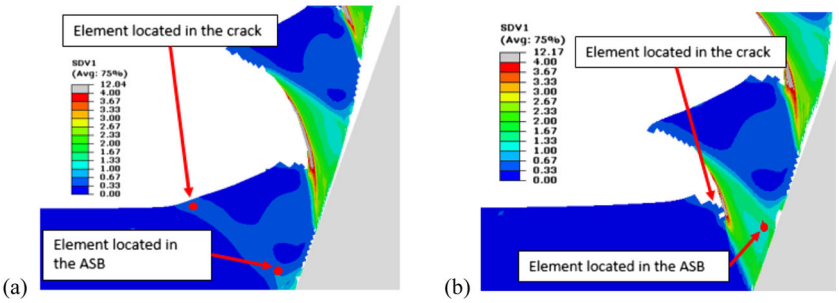

Fig. 9 Finite elements chosen in the crack and ASB areas. **a** Before segment formation and **b** after segment formation

value of plastic strain than the TANH model. This explains why the segmentation frequency is lower for hybrid model. Because the softening starts later for the hybrid model, the non-deformed area in the chip is more important and thus the segment size is more important. The consequence is that the frequency is lower. This is possible because of the criterion introduced through the critical strain ε_{crit}.

For a better comprehension of the chip formation process, the formation of a segment is observed in Fig. 8 and attention is paid to the damage variable (Fig. 8a, b) and temperature (Fig. 8e–h). The evolution of the damage variable shows that it increases faster near the tool tip and the chip free surface. These two locations seem to be where the damage mechanisms start first before propagating toward the center of the primary shear band. The fracture occurs at the chip free surface and propagates toward the tool tip. The analysis of the temperature field shows its concentration in the primary shear band, with a higher value at the tool tip where combined compression and shearing occur giving rise to a high plastic deformation energy converted to heat.

Two finite elements are chosen and analyzed: one is located inside the crack and another one in inward of the ASB, as indicated in Fig. 9. For each element, the plastic strain, recrystallization critical strain, temperature, and damage evolutions are plotted in Fig. 10. The evolution of the plastic strain of the recrystallized element, located in the ASB (Fig. 10a), shows that the DRX occurrence condition is reached. This can be related to the temperature evolution (Fig. 10b) which favors the critical strain decrease and temperature increase. The raise of temperature in the recrystallized element explains the low value of damage. On Fig. 10c, the condition for recrystallization occurrence is not reached for the element located in the crack. It should be noticed that the temperature is lower (Fig. 10d) in the crack than in the ASB. In the element located in the crack, the damage reached a value of 1 and then the complete failure of the element (Fig. 10d). In summary, the thermo-mechanical conditions during the formation of the chip are such that they enable recrystallization near the tool tip because of the high temperature while the damage mechanisms are favored at chip free surface.

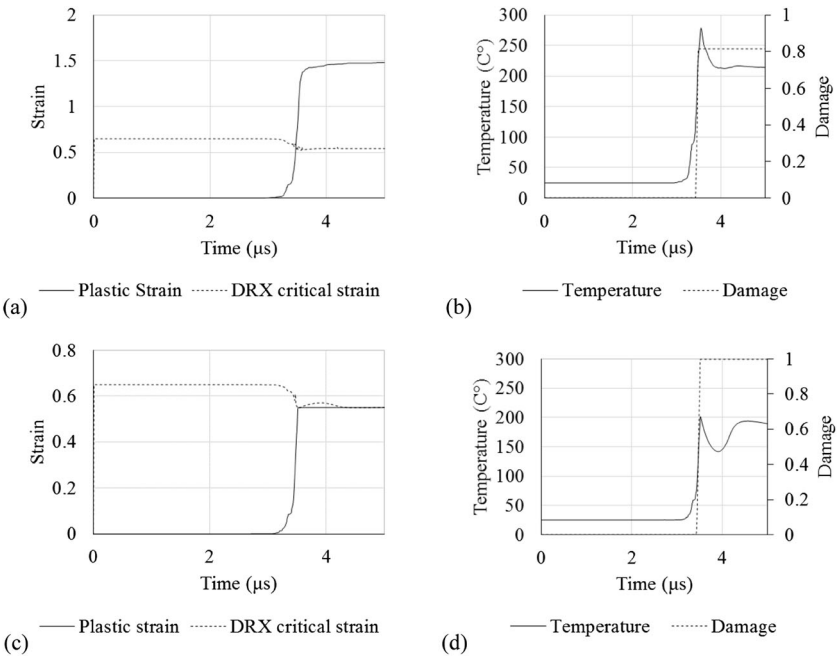

Fig. 10 Finite element located in ASB: **a** plastic strain and critical strain, and **b** temperature and damage. Finite element located in crack: **c** plastic strain and critical strain, and **d** temperature and damage

Table 9 Comparison between experimental and numerical mean values of cutting forces (V_c=30 m/min and f=0.28 mm/rev)

Case	F_C (N)
Hybrid model	341
TANH model	344
JC damage model	259
JC damage model with element deletion	238
Experimental [20]	386 ± 1

4.2 Analysis of the cutting forces

The cutting forces obtained from simulations are analyzed and compared to each other and to experimental results. The mean values of the predicted cutting forces of the four models are reported in Table 9. It can be seen that the predicted cutting force obtained with Hybrid model is the second better result after the TANH model result. There is a good accordance between the predicted value obtained with these two models and the experimental results. The JC damage models give very low value of cutting force.

Since the cutting forces obtained with the JC damage models (with and without FE deletion) are lower than the ones predicted by the hybrid and TANH models, the material damage induces a more important softening than the recrystallization process (see Fig. 7). In addition, the discontinuous chips induce the lowest cutting force. The cutting force oscillation caused by segmentation is reproduced by the all models (see Fig. 11). It is observable that the hybrid model shows a lower oscillation frequency in comparison to the other models. This result is in accordance with the segmentation frequency analyzed in Section 4.1.

This oscillation is related to the chip formation and the different phenomena occurring during the process, namely the formation of the adiabatic shear band and the crack initiation. The cutting force evolution during the formation process of a segment is analyzed in Fig. 12. A correlation is observed between the occurrence of each phenomenon and the value of the cutting force at the corresponding time. A segment formation is observed and three main steps are identified during this process: (i) The step (a): at this step, the cutting force is low and the formation of the crack 1 reaches its end. Since the material fracture is accompanied with a drop of the stress, the crack formation is in accordance with the cutting force decrease. (ii) The step (b): at this step, the cutting force is maximal and the formation of the peak of the segment is observed. The peak of the segment corresponds to the maximum of the chip thickness, so the material flow is also maximal at this moment. Since an important quantity of material is flowing, the segment peak formation is in accordance with the cutting force raise. (iii) The step (c): at this step, the cutting force is minimal and the formation of the crack 2 and the ASB is observed. The formation of the crack 2 and the ASB is accompanied by a strong softening of the material and a loss of rigidity, so the stress is minimal at this moment. Then the formation of the crack and the ASB is in accordance with the cutting force drop.

A correlation between the segmentation process and the cutting force oscillation is proposed by Atlati et al. [31]. A proposal is made concerning the mechanisms of chip formation that can be described in three steps: (i) in the first step, the tool affects the material and this allows the conditions of recrystallization to be reached near to the tool tip but not at the tool free surface. These conditions concern plastic strain, plastic strain rate, and temperature. Since the Ti-6Al-4V alloy has a low thermal conductivity, it promote the conditions of DRX occurrence to be reached because it is a thermally activated phenomenon. (ii) In the second step, DRX occurs and is accompanied

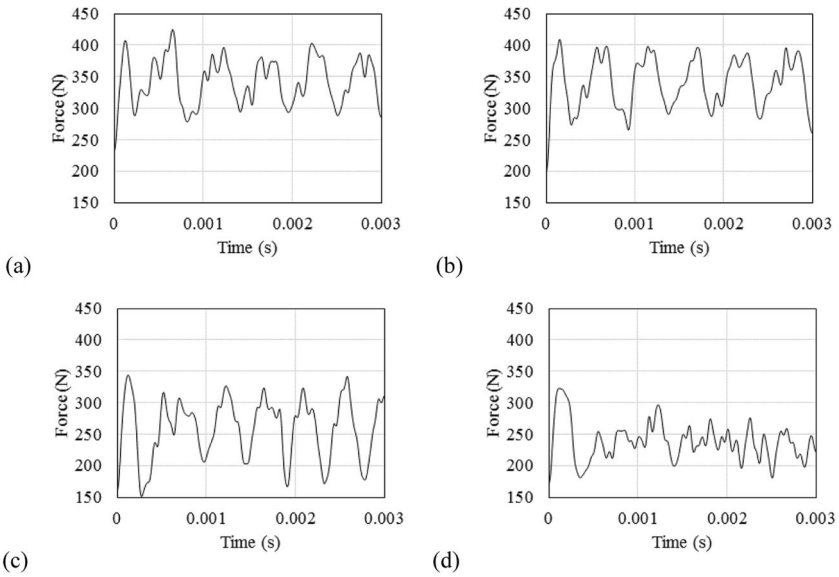

Fig. 11 Predicted cutting force for V_c=30 m/s and f=0.28 mm/rev: **a** hybrid, **b** TANH, **c** JC with JC damage, and **d** JC damage and element deletion models

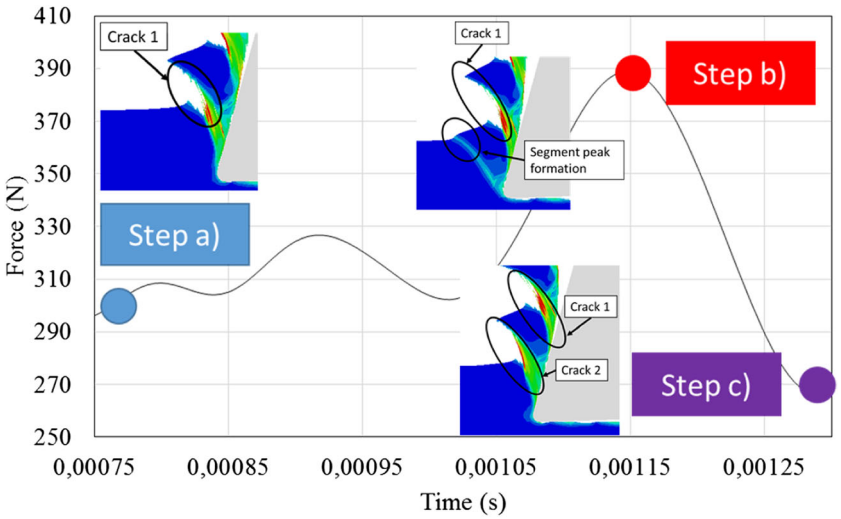

Fig. 12 Correlation between cutting force evolution and chip formation process (chip segment formation)

by a severe plastic deformation inward the ASB and damage occurs near the chip free surface in the ASB giving rise to a crack. (iii) Finally, the third step is the formation of the segment because of the difference of rigidity between the recrystallized areas and the non-recrystallized areas of the chip.

4.3 Analysis of the cutting speed effect

Two other cutting conditions are simulated in order to analyze the response of the proposed Hybrid model (V_c=60 and 120 m/min, with f=0.28 mm/rev). Figure 13 shows that the damage mechanism is intensified when cutting speed increases. The fracture in the ABS is accentuated, giving rise to fragmented chips at higher cutting speed. As the cutting speed increases, the fracture length in the ABS increases up to separate completely the chip along its thickness. This is due the increase of the strain rate in the ASB with cutting speed. Indeed, the fracture strain decreases when the strain rate increases and therefore the fracture occurs earlier, meaning for less plastic deformation in the ASB. It is thus considered that the effect of the strain rate is more dominant than the one of thermal softening as cutting speed increases. This tendency was also observed by Ma et al. [32] for higher cutting speed (between 90 m/s and 210 m/s in the case of cutting with light gas gun).

5 Conclusion

A physical behavior model based on recrystallization and damage mechanisms is proposed to obtain an accurate prediction of the Ti-6Al-4V cutting process.

(1) The material has a different behavior according to the thermo-mechanical conditions in the chip.
(2) Both damage and DRX induce chip segmentation by lowering the flow stress. However, these two mechanisms cannot occur simultaneously at the same material point since recrystallization impedes damage mechanisms.
(3) The JMAK model is used to introduce a DRX initiation criterion depending on the thermo-mechanical conditions.
(4) The material near the tool tip and inward of the ASB undergoes DRX and severe plastic deformation due to high temperature, while near the chip free surface in the

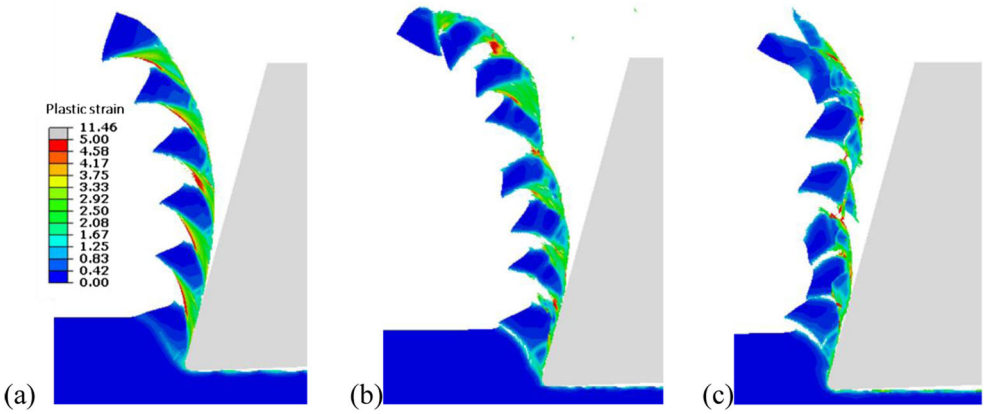

Fig. 13 Effect of the cutting speed on the chip formation as reproduced with the hybrid model: f=0.28 mm/rev and V_c(m/min) = 30 (**a**), 60 (**b**), and 120 (**c**)

ASB it undergoes damage and fracture because the temperature is lower.

(5) The Hybrid model was compared to JC model with and without damage and to TANH model, and to an experimental data. The comparison tends to confirm that the hybrid model reproduces more accurately the chip morphology. This confirms the assumptions made, concerning the behavior of the hard Ti-6Al-4V alloy.

(6) The analysis of the cutting conditions effect on the chip morphology with the hybrid model shows a transition from segmented chips with partial fracture to fragmented chips as cutting speed increases.

References

1. Donachie MJ (2000) Titanium: a technical guide. ASM International, Ohio
2. Sun S, Brandt M, Dargusch MS (2009) Characteristics of cutting forces and chip formation in machining of titanium alloys. Int J Mach Tools Manuf 49:561–568
3. Su G, Liu Z, Li L, Wang B (2015) Influences of chip serration on micro-topography of machined surface in high-speed cutting. Int J Mach Tools Manuf 89:202–207
4. Altintas Y (2012) Manufacturing automation: metal cutting mechanics, machine tool vibrations, and CNC design. Cambridge university press, Cambridge
5. Cheng K (2008) Machining dynamics: fundamentals, applications and practices. Springer Science & Business Media, Berlin
6. Jaspers S, Dautzenberg JH (2002) Material behaviour in metal cutting: strains, strain rates and temperatures in chip formation. J Mater Process Technol 121:123–135
7. Nakayama K, Arai M, Kanda T (1988) Machining characteristics of hard materials. CIRP Ann.-Manuf. Technol. 37:89–92
8. Shaw MC, Vyas A (1993) Chip formation in the machining of hardened steel. CIRP Ann.-Manuf. Technol. 42:29–33
9. Umbrello D (2008) Finite element simulation of conventional and high speed machining of Ti6Al4V alloy. J Mater Process Technol 196:79–87
10. Aurich JC, Bil H (2006) 3D finite element modelling of segmented chip formation. CIRP Ann.-Manuf. Technol. 55:47–50
11. Zhen-Bin H, Komanduri R (1995) On a thermomechanical model of shear instability in machining. CIRP Ann-Manuf Technol 44:69–73
12. Davies MA, Burns TJ, Evans CJ (1997) On the dynamics of chip formation in machining hard metals. CIRP Ann.-Manuf. Technol. 46:25–30
13. Wan ZP, Zhu YE, Liu HW, Tang Y (2012) Microstructure evolution of adiabatic shear bands and mechanisms of saw-tooth chip formation in machining Ti6Al4V. Mater Sci Eng A 531:155–163
14. Sagapuram D, Viswanathan K, Mahato A, Sundaram NK, M'Saoubi R, Trumble KP, Chandrasekar S (2016) Geometric flow control of shear bands by suppression of viscous sliding, in: Proc R Soc A, The Royal Society: p. 20160167
15. Nouari M, Makich H (2013) Experimental investigation on the effect of the material microstructure on tool wear when machining hard titanium alloys: Ti–6Al–4V and Ti-555. Int J Refract Met Hard Mater 41:259–269
16. Rhim S-H, Oh S-I (2006) Prediction of serrated chip formation in metal cutting process with new flow stress model for AISI 1045 steel. J Mater Process Technol 171:417–422
17. Calamaz M, Coupard D, Girot F (2008) A new material model for 2D numerical simulation of serrated chip formation when machining titanium alloy Ti–6Al–4V. Int J Mach Tools Manuf 48:275–288
18. Liu R, Melkote S, Pucha R, Morehouse J, Man X, Marusich T (2013) An enhanced constitutive material model for machining of Ti–6Al–4V alloy. J Mater Process Technol 213:2238–2246
19. Sima M, Özel T (2010) Modified material constitutive models for serrated chip formation simulations and experimental validation in machining of titanium alloy Ti–6Al–4V. Int J Mach Tools Manuf 50:943–960
20. Ducobu F, Rivière-Lorphèvre E, Filippi E (2016) Material constitutive model and chip separation criterion influence on the modeling of Ti6Al4V machining with experimental validation in strictly orthogonal cutting condition. Int J Mech Sci 107:136–149
21. Atmani Z, Haddag B, Nouari M, Zenasni M (2016) Combined microstructure-based flow stress and grain size evolution models for multi-physics modelling of metal machining. Int J Mech Sci 118:77–90
22. Follansbee PS, Kocks UF (1988) A constitutive description of the deformation of copper based on the use of the mechanical threshold stress as an internal state variable. Acta Metall 36:81–93
23. Zerilli FJ, Armstrong RW (1987) Dislocation-mechanics-based constitutive relations for material dynamics calculations. J Appl Phys 61:1816–1825
24. Arısoy YM, Özel T (2015) Prediction of machining induced microstructure in Ti–6Al–4V alloy using 3-D FE-based simulations: effects of tool micro-geometry, coating and cutting conditions. J Mater Process Technol 220:1–26
25. Pan Z, Liang SY, Garmestani H, Shih DS (2016) Prediction of machining-induced phase transformation and grain growth of Ti-6Al-4 V alloy. Int J Adv Manuf Technol 87:859–866
26. Shang X, Cui Z, Fu MW (2017) Dynamic recrystallization based ductile fracture modeling in hot working of metallic materials. Int J Plast 95:105–122
27. Kolmogorov VL, Smirnov SV (1998) The restoration of the margin of metal plasticity after cold deformation. J Mater Process Technol 74:83–88
28. Smirnov SV (2013) The healing of damage after the plastic deformation of metals, Frat Ed Integrità Strutt 7
29. Wang B, Liu Z (2015) Shear localization sensitivity analysis for Johnson–Cook constitutive parameters on serrated chips in high speed machining of Ti6Al4V. Simul Model Pract Theory 55:63–76
30. Kouadri S, Necib K, Atlati S, Haddag B, Nouari M (2013) Quantification of the chip segmentation in metal machining: application to machining the aeronautical aluminium alloy AA2024-T351 with cemented carbide tools WC-Co. Int J Mach Tools Manuf 64:102–113
31. Atlati S, Haddag B, Nouari M, Zenasni M (2011) Analysis of a new segmentation intensity ratio "SIR" to characterize the chip segmentation process in machining ductile metals. Int J Mach Tools Manuf 51:687–700
32. Ma W, Chen X, Shuang F (2017) The chip-flow behaviors and formation mechanisms in the orthogonal cutting process of Ti6Al4V alloy. J Mech Phys Solids 98:245–270